Two-Way Reversible Shape Memory in a Semicrystalline Network

Taekwoong Chung,[†] Angel Romo-Uribe,[‡] and Patrick T. Mather*,[†]

Department of Macromolecular Science and Engineering, Case Western Reserve University, 2100 Adelbert Road, Cleveland, Ohio 44106, and Instituto de Ciencias Fisicas, Universidad Nacional Autonoma de Mexico Cuernavaca, Morelos 62210, Mexico

Received July 9, 2007; Revised Manuscript Received October 25, 2007

ABSTRACT: Cooling-induced crystallization of cross-linked poly(cyclooctene) films under a tensile load results in significant elongation and subsequent heating to melt the network reverses this elongation (contracting), yielding a net two-way shape memory (2W-SM) effect. The influence of cross-linking density on the thermal transitions, mechanical properties, and the related 2W-SM effect was studied by varying the concentration of cross-linking agent dicumyl peroxide (DCP) and using differential scanning calorimetry (DSC), gel fraction measurements, dynamic mechanical analysis (DMA), and customized 2W-SM analysis. The latter showed that there is crystallization-induced elongation on cooling and melting-induced shrinkage on heating (2W-SM), with lower cross-link density leading to higher elongation at the same applied stress. For a given cross-link density, however, increasing the tensile stress applied during cooling resulted in greater stress-induced crystallization. We further observed that the onset temperatures for elongation on cooling (T_c) and contraction on heating (T_m) shifted to higher temperatures with decreasing cross-link density. Similarly, the degree of molecular orientation achieved upon deformation was found to increase with decreasing cross-link density. The impact of stress on the 2W-SM effect was examined using wide-angle X-ray diffraction (WAXD), revealing a transition from bimodal to unimodal orientation. As the crystalline structure evolves from bimodal (low stress) to unimodal (high stress), the crystallization occurs along a single preferred orientation thus inducing greater elongation along the stretching direction. We anticipate that the observed 2W-SM property in a semicrystalline network will enable applications heretofore possible only with costly shape memory alloys and liquid crystalline elastomers.

Introduction

Shape memory polymers (SMPs) are an exciting class of smart materials that offer the capacity to undergo large and rapid shape changes under specific and tailored environmental conditions.[1−3] So-called "one-way" shape memory polymers (1W-SMPs) feature an equilibrium (permanent) shape, dictated by cross-linking, that can be deformed at either ambient or elevated temperatures, "fixed" to a temporary and dormant shape and then recovered to a stress-free condition by heating or otherwise liberating chain mobility constraints. Uniquely, SMPs allow molecular design of tailored stiffness and responsiveness to external stimuli such as heat, pH, electricity, and light. Many studies have been performed and reported with a variety of SMPs such as phase separated polyurethanes,[4,5] cross-linked polyethylene,[6] polynorbonene,[7] styrene−butadiene copolymers,[8] and biodegradable shape memory polymers based on oligo (ϵ-caprolactone).[9] It has been well-documented that heat-sensitive 1W-SMPs can have their stiffness and critical temperature tailored through compositional variations that control crystallinity, the melting temperature (T_m), and/or the glass transition temperature (T_g). Despite the breadth of 1W-SMP compositions, the number of two-way shape memory polymer examples is comparatively small, heretofore being limited to the liquid crystalline elastomer family. This is discussed more below.

In contrast to SMPs, metallic shape memory alloys (SMAs) feature a shape change stimulated by a modest temperature crystal−crystal (martensite−austenite) transition. Furthermore, it is well-known that a specific thermomechanical treatment, called "training", plays a critical role in obtaining a two-way shape memory behavior from an initial one-way shape memory alloy. While the native one-way shape memory alloy can only "remember" the high-temperature shape, the trained two-way shape memory alloy can "remember" both high and low-temperature shapes through the creation of a dislocation network. In comparison to the tensile strains achievable with the SMA-based one-way shape memory effect ($\sim$ 8%) reversible strains of only 4% are possible[10] for the two-way shape memory effect and one must resort to geometric strain amplification, as in the form of a helical spring or bimorph, to achieve reasonable actuation strokes. Interestingly, reports exist of composite structures in which an elastomeric polymer is embedded with SMA wires to yield, following training, a beam with reversible flexural actuation capacity.[11,12] In our work, we seek to develop similar functionality but without the complexity of composite material fabrication.

Demand has arisen for *reversible actuation* in polymers, especially for artificial muscles or actuators.[13,14] Toward this end, a wide range of materials have been investigated to varying degrees of success, including the modulated gel technique,[15] electroactive polymers,[16−18] conducting polymers,[19−22] and liquid crystalline elastomers (LCEs).[13,14,23,24] Among these candidates, LCEs have shown the best potential based on their fast actuation speed and mechanical properties that can be tuned and optimized to mimic skeletal muscle. Two-way shape memory in LCEs features reversible actuation at a single, generally nonzero, applied stress. In particular, with a tensile stress applied, elongation is observed during cooling from the isotropic to liquid crystalline phase, while contraction is observed upon heating throught the same phase transition. The surprising elongation upon cooling is attributed to a distinct "soft

* To whom correspondence should be addressed. Present address: Syracuse Biomaterials Institute and Biomedical and Chemical Engineering Department, 121 Link Hall, Syracuse University, Syracuse, NY 13244. E-mail: ptmather@syr.edu. Phone: 315-443-8760. Fax: 315-443-9175.
† Case Western Reserve University.
‡ Universidad Nacional Autonoma de Mexico Cuernavaca.

10.1021/ma071517z CCC: $40.75
Published on Web 12/13/2007

elasticity" characteristic of the liquid crystalline phase,[25] while heating induced contraction is a simple consequence of achieving the strain associated with tensile modulus of the isotropic elastomer. The effect is quite dramatic: under a small preload stress of 6 kPa, a recoverable strain as high as 300% was observed when traversing the isotropic−nematic transition monodomain samples.[26] The reversible actuation behavior in liquid crystalline elastomers have been demonstrated by Finkelman and others in the form of side-chain LCE architecture.[14,27−29] In addition to side-chain liquid crystalline elastomers, recently main-chain liquid crystalline elastomers have attracted interest due to their intrinsically high, yet liable, orientational order and network strain compared to the side chain analogue.[29,30] Despite their attractive characteristics, LCEs take multiple steps to synthesize so that they are intrinsically expensive to produce. Materials with similar characteristics are needed but with a simpler synthetic protocol for their production.

In prior work, we reported the synthesis of a 1W-SMP, poly(cyclooctene) (PCO), by facile ring opening metathesis polymerization (ROMP) of cyclooctene using a Grubb's catalyst.[31] The PCO was then covalently cross-linked by peroxide cure to form a semicrystalline thermoset polymer possessing a melting temperature easily adjusted through cross-linking density and trans/cis composition in vinylene groups. As a 1W-SMP, excellent fixing to a temporary shape on cooling as well as rapid recovery to the original, stress-free, shape on heating was observed.[31] To our surprise, we have found that the same materials exhibit significant two-way shape memory behavior and this behavior was recently investigated and reported herein. Moreover, a commercial source for poly(cyclooctene) with properties similar to our version was identified under the tradename Vestenamer. In this study, we report on the preparation and characterization of a simple composition exhibiting two-way shape memory behavior: cross-linked PCO. In a manner similar to LCEs discussed above, cross-linked PCO exhibits tensile elongation upon cooling and complete tensile contraction on heating under a constant stress. The thermally reversible two-way shape memory behavior was characterized using a dynamic mechanical analyzer (DMA) as a function of applied stress as well as the extent of cross-linking of PCO. In addition, the crystalline structure was investigated using wide-angle X-ray diffraction (WAXD) in order to elucidate the origin of cooling-induced expansion and heating induced contraction.

Experimental Section

Sample Preparation. Poly(cyclooctene) (Degussa Corporation, Vestenamer 8012 with a trans content of 80%) and dicumyl peroxide (DCP) (>98% purity, Aldrich) were used as received. All specimens were prepared using a microcompounder (DACA) and a Carver press (model C) as revealed in the following processing protocol example. The microcompounder was first preheated to 80 °C and equilibrated for at least 5 min to ensure a uniform temperature distribution within the whole chamber. The dried PCO pellets were next fed into the chamber and mixed with DCP with different amounts to obtain the desirable composition in the final products for 5 min at a rotation speed of 50 rpm. Such a process is capable of melting the polymer and uniformly dispersing the peroxide, without inducing significant cross-linking. The mixture was then extruded from the microcompounder and cooled to room temperature. After adding into a spacer frame made of Teflon (thickness: 0.4 mm), the extrudate was pressed between two hot plates preheated to 180 °C and then cured for 30 min under a load more than sufficient to seal the mold periphery (1000 lb). The fully cured samples were cooled to room temperature. The DCP content varied from 1 wt % to 2 wt % based on the weight of PCO.

Gel Fraction Measurement. To determine the quality of cross-linking, network gel fraction values of the cross-linked PCO samples were measured using extraction and gravimetry. Each PCO sample was extracted using boiling THF (a good solvent for linear PCO) in a Soxhlet extraction apparatus for 24 h and then vacuum-dried at 50 °C to remove residual solvent for calculation of gel fraction. Gel fraction values were calculated using the initial dry weight, before extraction, W_i, and the dry weight after extraction, W_d,

$$G(\%) = \frac{W_d}{W_i} \times 100\% \tag{1}$$

For polymers featuring favorable interactions with THF, this quantity ranges from 0% for a polymer completely soluble in THF to 100% for a perfect network; i.e., a network featuring no free polymer chains.

Thermal Analysis. Thermal properties were measured using differential scanning calorimetry (DSC, TA Instruments, Inc., model Q100). The samples were heated at a rate of 10 °C/min from −50 to 100 °C and were then cooled to −50 °C at a cooling rate of 10 °C/min. Subsequently, a second heating run at the same rate of 10 °C/min was executed to 100 °C. The observed melting temperature (T_m) of each cross-linked PCO sample was determined from the second heating curve. The melting temperatures and heats-of-fusion were evaluated from the peak and the areas of maxima of the appropriate endotherms.

Shape Memory and Dynamic Mechanical Analysis. A Perkin-Elmer dynamic mechanical analyzer (DMA-7e) was used with multiple configurations to explore and analyze one-way and two-way shape memory behavior, as well as the usual linear viscolastic properties. Samples with different degrees of cross-linking (as controlled by DCP content) were cut into rectangular strips with dimensions of 0.4 mm × 2.0 mm × 15.0 mm. Each PCO strip was placed in tension between a fixed and movable clamp. One-way shape memory behavior was characterized using a four-step program that begins at elevated temperature ($T > T_m$). (1) Deformation: the PCO strip is elongated by increasing the applied load from 0 to 0.38 N at a rate of 0.05 N/min and at $T = 75$ °C. (2) Fixing: the sample is then cooled at 2 °C/min to a temperature below T_m under constant load, this step was found to fix the temporary shape quite completely. (3) Unloading: the load was removed at a constant rate of 0.1 N/min, revealing the quality of fixing through the resulting final strain. (4) Recovery: Finally, heat-induced recovery toward the original length was examined by heating to a temperature above T_m at a rate of 2 °C/min.

In contrast, the two-way shape memory cycle is conducted with the following three steps, the only difference being the lack of an unloading step prior to reheating. (1) Deformation: The sample is stretched at high-temperature ($>T_m$) by increasing the applied load from x to y at 0.05 N/min. (2) Cooling: The deformed and loaded sample is then cooled to low temperature ($<T_c$) at a rate of 2 °C/min. (3) Heating: After being held for 10 min at 15 °C, the sample is then heated to 100 °C at a rate of 2 °C/min while the sample length is measured. This thermomechanical protocol was performed repeatedly by cooling and heating under a constant applied tensile stress. Characteristics of the 2W-SM behavior include the actuation magnitude, $R_{act}(\sigma)$ and the strain recovery magnitude (R_{rec}). $R_{act}(\sigma)$ is the strain increment during actuation, expressed as a percentage of the baseline strain at $T > T_m$. These characteristics are calculated from the observable sample lengths for a two-way shape memory behavior as follows.

$$\begin{aligned} R_{act}(\sigma) &= \Delta\epsilon \times 100\% \\ &= (\epsilon_{low}(\sigma) - \epsilon_{high}(\sigma)) \times 100\% \\ &= \frac{L_{low}(\sigma) - L_{high}(\sigma)}{L(0)} \times 100\% \end{aligned} \tag{2}$$

$$R_{rec}(\sigma) = \frac{L_{low} - L_{high}^{final}}{L_{low} - L_{high}^{initial}} \times 100\% \tag{3}$$

Table 1. Characterization DCP-Cured PCO Samples

sample[a]	DCP wt %	T_m (°C)	T_c (°C)	ΔH (J/g)	χ_C (%)[b]	G (%)[c]	R_r[d] (%)	E' (80 °C) (MPa)[e]
PCO-D1.0	1	48.2	28.7	61.0	28.2	85.0	93.5	0.93
PCO-D1.25	1.25	45.7	27.6	60.1	27.8	90.1	96.0	1.28
PCO-D1.5	1.5	44.6	26.6	57.9	26.8	92.3	97.5	1.49
PCO-D1.75	1.75	43.7	25.9	57.1	26.4	93.6	98.2	1.63
PCO-D2.0	2	41.9	24.2	55.5	25.7	94.1	99.0	2.01

[a] Cross-linked PCO nomenclature indicates DCP weight percent as the suffix. [b] Crystallinities were determined from $\Delta H_{crystal} = 216$ J/g.[37] [c] G: Gel fraction. [d] R_r: Strain recovery ratio. [e] Storage modulus at 80 °C.

For eq 2, L_{high} is the length of the sample at high-temperature ($T > T_m$) and L_{low} is the length at low temperature ($T < T_m$), both with stress, σ, applied. For eq 3, $L_{high}^{initial}$ is the original length under stress and at a high temperature, while L_{high}^{final} is the final length under stress after reheating to induce recovery.

For conventional DMA characterization, the tensile storage modulus (E') was recorded at a heating rate of 2 °C/min using an oscillation frequency of 1 Hz and a temperature range −80 °C < T < 100 °C. To remove thermal history prior to such DMA measurements, samples were first heated in a vacuum oven at 100 °C for approximately 10 min and then cooled slowly to room temperature.

Wide-Angle X-ray Diffraction. Ex situ wide-angle X-ray diffraction measurements were employed to aid in the elucidation of the observed thermomechanical response at the microstructural level. In particular, following steps 1 and 2 of the 1W-SM protocol detailed above, samples were collected from the DMA apparatus and then mounted on the sample support of a Statton camera WAXD apparatus with the length and width axes perpendicular to the beam, vertical and horizontal, respectively. A calibrated sample−detector distance of 7.40 cm was employed, and X-ray diffraction patterns were recorded on a Fuji image plate measuring 10 cm × 15 cm and processed with a digital reader (Fuji, FDL 5000) to yield pixels of dimension 25 μm square. The X-ray patterns were analyzed using the image analysis software ImageTool v 3.0 (UTHSCSA). Additional X-ray powder diffraction patterns (Rigaku RINT2200 diffractometer) were obtained with Ni-filtered Cu K_α radiation ($\lambda = 1.54068$ Å) generated at 30 kV and 30 mA with diffracted radiation collected at a scanning speed of 0.5°2θ/min in the range of 1−40°2θ and then analyzed using MDI (Jade version 5) software.

Results and Discussion

Poly(cyclooctene), PCO, is a semicrystalline polyolefin with some unique properties when compared to the more commonly studied polyethylene and polypropylene. For example, PCO features unsaturation, a carbon−carbon double bond, at precisely every eighth carbon. This offers potential for facile cross-linking. In addition, the cis/trans ratio of the same carbon−carbon double bond bears influence on the degree of crystallinity and melting temperature, greater trans levels yielding greater crystallinity. Finally, for shape memory purposes, the melting temperature is conveniently close to room temperature ($T_m \sim 55$ °C), but high enough to allow rapid crystallization at room temperature. We prepared a set of chemically cross-linked PCO films using DCP as a thermal initiator to investigate shape memory properties, especially, two-way shape memory behavior. For a DCP range of 1−2%, we obtained gel fraction values from 85% to 94%, with the gel fraction, G, increasing monotonically with DCP content as expected. The results are summarized in Table 1 along with other characterization data to be described later. While not a direct measure of cross-linking degree, rubber modulus data will be described below, the values do indicate quite complete cross-linking in the sense of incorporating all constituent chains in the percolating network. We now proceed to describe the basic thermal and mechanical properties.

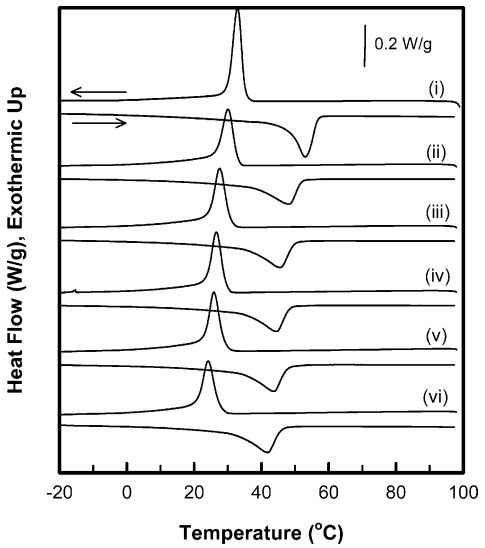

Figure 1. First cooling and second heating DSC thermograms of PCO cured with various amounts of DCP: (i) pure PCO (ii) 1%, (iii) 1.25%, (iv) 1.5%, (v) 1.75%, and (vi) 2%. The constant heating and cooling rate of 10 °C/min was used. Upper and bottom line in a pair of DSC traces indicate first cooling and second heating, respectively.

Thermal and Mechanical Properties. PCO samples cured with DCP "melt" to a stable rubbery plateau above T_m that is void of macroscopic flow, allowing reversible (elastic) deformations up to several hundred percent without flow (Supporting Information), as will be revealed with DMA data, below. The melting temperature (T_m), only slightly modified from the linear polymer, as we shall show, acts as the transition temperature to trigger a shape memory behavior of the networks. For 1W-SM response, cooling below T_m leads to crystallization that serves as the fixing mechanism of deformed PCO samples, while heating above T_m leads to chain mobility that allows strain recovery to mechanical equilibrium in accordance with the applied load. As previously reported,[31] cross-linking of PCO with DCP has a critical influence on physical properties such as the melting and crystallization temperatures, T_m and T_c, respectively, melting enthalpy, and mechanical properties, all of which we have investigated.

In order to evaluate the possibility of tuning the transition temperatures (i.e., T_m and T_c) by cross-linking extent, melting and crystallization thermograms obtained using differential scanning calorimetry (DSC) for PCO samples cured with different DCP concentrations were conducted. The results are shown in Figure 1 with analysis data summarized in Table 1. One sees immediately that cross-linking PCO does not qualitatively alter the melting and recrystallization behavior relative to linear PCO, at least not for 1−2 wt % DCP. Instead, quantitative alterations result. Inspection of Figure 1 and Table 1 reveals that the transition temperatures, T_m and T_c, along with associated latent heats of melting and crystallization (heat of fusion), modestly decrease with increasing DCP concentration. In particular, the heat of fusion decreases by ∼7% on increasing the DCP content from 1 to 2%. We attribute this trend to a constraining effect of cross-link junctions on crystal growth, specifically the local chain mobility necessary for chain insertion into a growing crystal is suppressed in the neighborhood of a cross-link site. This hypothesis is supported by the reduction in melting enthalpy with DCP content, resulting in the reduction of crystallinity (Table 1). Indeed, we have reported in the past a significant alteration in the crystallization kinetics of PCO due to cross-linking.[32] Similar findings have been reported for the cross-linking of polypropylene[33] and polyethylene.[34,35]

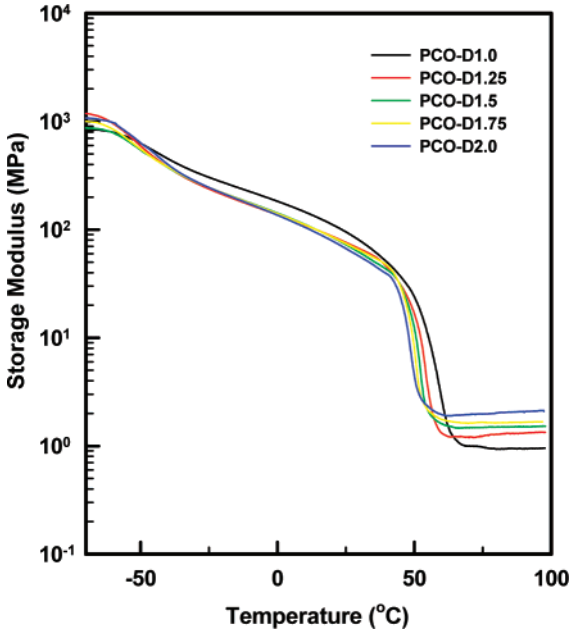

Figure 2. Storage modulus (E') vs temperature for the cross-linked PCOs as a function of the added DCP in amounts shown. E' was recorded at a heating rate of 2 °C/min with frequency of 1 Hz.

From the standpoint of shape memory behavior, increasing the degree of cross-linking (via increased DCP content) may simultaneously increase the rubber modulus, enhancing work capacity during strain recovery, while the degree of crystallinity is reduced (as indicated by the heat of fusion alteration discussed above), possibly hampering strain fixing.[31] To shed light on such a tradeoff, dynamic mechanical analyses were conducted for the series of cross-linked PCO samples. Shown in Figure 2 are the tensile storage modulus (E') traces plotted as a function of temperature for samples spanning the same range of DCP contents as for the thermal analysis. In the low-temperature region, we clearly observe the glass rubber transition near $T = -70$ °C where the tensile storage moduli drop from approximately 1 GPa to a sloped plateau beginning at approximately 300 MPa (leatherlike) and falling to approximately 50 MPa (stiff elastomer) just prior to the melting transition. Consistent with our observed slight decrease in crystallinity on increasing DCP content (Table 1), the tensile storage modulus for $T_g < T < T_m$ is also seen to decrease, most dramatically from 1.0% (PCO-D1.0) to 1.25% (PCO-D1.25). Upon traversing the melting transition for each network sample, the tensile storage modulus drops sharply, reaching an extended rubbery plateau above T_m whose modulus value depends sensitively on DCP content and may serve as a measure of cross-linking density. These values are summarized in Table 1 and range from 0.9 to 2 MPa, a range typical for cross-linked elastomers and coincidentally close in numerical value to DCP content in wt %. As anticipated from DSC findings, the onset temperature corresponding to the modulus drop shifted to lower temperature with increasing DCP content.

In our prior report,[31] it was found that cross-linking PCO with too low a concentration of DCP led to viscous flow above T_m while cross-linking of too high a DCP content undesirably broadened the melting and crystallization transitions, impacting one-way shape memory behavior. Though for different reasons than one-way shape memory, two-way shape memory behavior is also impacted by cross-linking, through both the rubber modulus and melting transition. Indeed, the narrow range of 1−2 wt % was selected from prior experience[31] to afford both a flat rubber plateau and narrow melting transition. For lower cross-linking densities (0.5 wt % DCP), significant creep occurs above T_m, while for higher cross-linking densities (3 wt % DCP) the melting transition excessively broadens.

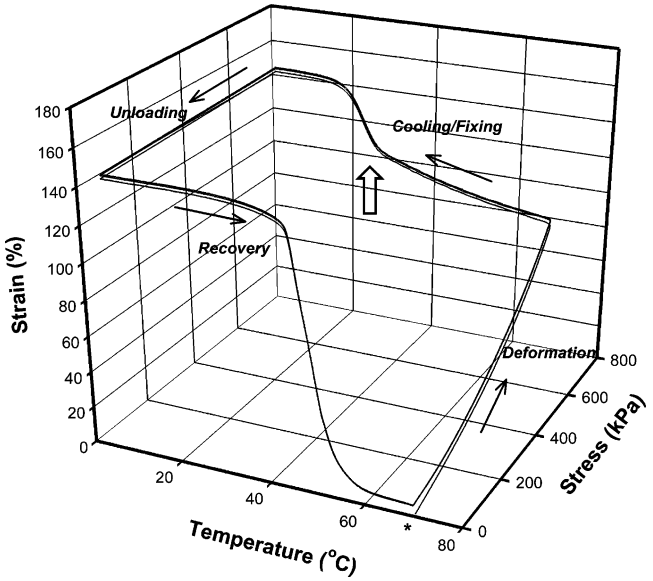

Figure 3. One-way shape memory cycles for PCO-D1.5. The asterisk indicates the beginning of the experiment. The sample is deformed by increasing stress at 75 °C. Cooling (2 °C/min) and removing stress yield a temporary fixed shape. Shape recovery of the original equilibrium shape is obtained by heating (2 °C/min).

Shape Memory Properties. As described in the Experimental Section, a dynamic mechanical analyzer was used in controlled force and static mode to characterize precisely the one- and two-way shape memory effect of the cross-linked PCO samples. Figure 3 shows repeated one-way shape memory cycles for PCO-D1.5. Here, the sample was elongated up to 80% at a high-temperature (75 °C) above T_m (the deformation step) and cooled down to 5 °C at a constant cooling rate (2 °C/min). At low temperature, the temporary shape was obtained and the applied load was removed. The PCO sample recovered the original shape due to entropic elasticity upon heating back to the high-temperature (75 °C) at a constant rate (2 °C/min). The cycle was repeated three times following the same thermomechanical protocol. Although there exists a slight slipping of the sample from the DMA's clamp during the first cycle, remarkably reproducible shape memory behavior is observed from one cycle to the next. Thus, it is clear that such a cross-linked PCO (Ventenamer 8012) sample exhibits an excellent one-way shape memory property, accompanied by both good fixing and recovery. These results are similar to those previously reported for a PCO prepared by us via ring-opening polymerization.[31] Quite interestingly, it was observed that a remarkable *increase in strain* occurred during cooling as indicated by the bold arrow (Figure 3), at a temperature corresponding to PCO crystallization as observed with DSC (Figure 1). This result indicated to us that the cured PCO materials have potential of two-way shape memory behavior, which requires an elongation event on cooling. On the basis of this result, we explored two-way shape memory behavior of the cured PCOs (simply removing the low-temperature unloading step), which involves pre-deformed samples reversibly elongating and contracting on cooling and heating through the transition temperature, respectively.

Two-way shape memory behavior of PCO samples cross-linked with different DCP amounts are shown in Figure 4, where the strain *increment* ($R_{act}(\sigma)$, eq 2) is plotted versus temperature. The cured PCO samples were initially in a stress-free state.

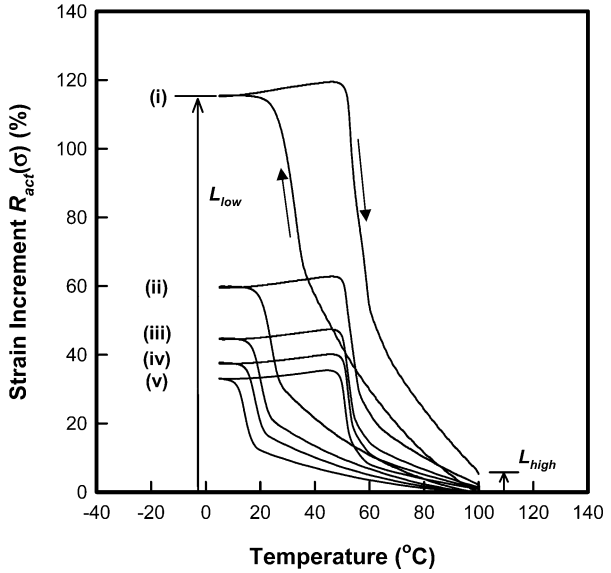

Figure 4. Two-way shape memory behavior of PCOs cured with different DCP contents: (i) 1.0, (ii) 1.25, (iii) 1.5, (iv) 1.75, and (v) 2.0 wt %. The samples were elongated at high-temperature (100 °C) under a constant stress of 600 kPa. The deformation step is followed by a cooling process (2 °C/min), inducing an increase in strain. Then, the increased strain decreases by a heating process (2 °C/min) to high temperature.

Then, the samples were elongated under a constant stress at an elevated temperature (100 °C). Since the cooling and heating rates have a significant impact on the shape memory behavior, a constant heating and cooling rate of 2 °C/min was maintained for all samples. Taking into consideration that the length of the pre-deformed sample at high temperature is the initial length ($R_{act}(\sigma) = 0\%$), the change in $R_{act}(\sigma)$ with temperature was observed through cooling and heating.

During the cooling step, we observe that strain slightly increases with decreasing temperature, but at the point of crystallization the strain *increases* quite dramatically with an increment, $R_{act}(\sigma) \sim 25\%$ for the applied stress values studied. (Note: Supporting Information includes graphs of the total actual strain, ϵ, not the strain increment, versus temperature.) At first glance, this is surprising since according to the linear viscoelastic measurements (at small strain) shown in Figure 2 the elastic modulus is significantly *higher* below T_m than above. Thus, from elastic modulus (linear) considerations alone, one expects a strain *decrease* on cooling below T_m at constant tensile stress. That we see the opposite is indication of a nonlinear, large strain effect not ascertained with linear viscoelastic measurements. The dependence on degree of cross-linking is also seen clearly in Figure 4: the strain increment dramatically increases with decreasing DCP concentration when examined at the same applied tensile stress. This finding seems reasonable, as the cross-link junctions impose constraint against continued sample deformation in a manner similar to the modulus-cross-link density relationship of rubber elasticity. Further, we see from Figure 4 that for a fixed tensile stress of 600 kPa, T_m increases slightly while T_c increases dramatically as cross-linking is decreased.

By the coincidence of temperatures at which the cooling-induced elongation and crystallization events occur, we reason that the increase in strain is due to the crystallization event, itself, which differs significantly from the no-stress case where no macroscopic deformation (other than isotropic contraction due to density increase) is witnessed. During cooling under stress, but prior to crystallization, the elongated amorphous network chains (stretched Gaussian coils) adjust their junction−junction distance slightly but suddenly increase in this dimension upon crystallizing at constant stress. Surely this involves a decrease in configurational entropy as is the case for quiescent polymer crystallization but even more so if chain folding into lamellae is diminished in deference to a more extended-chain crystalline configuration.

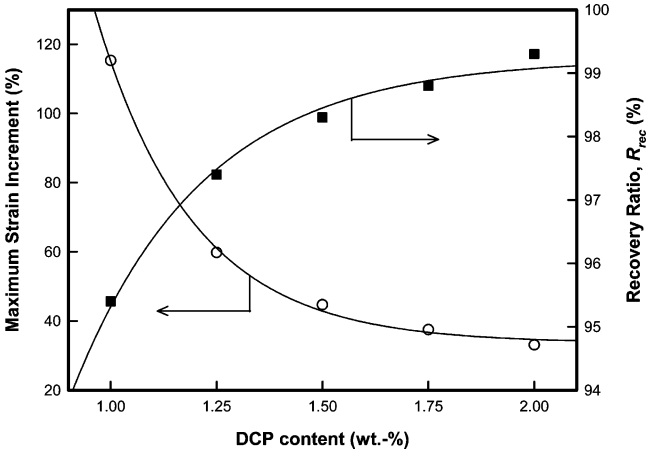

Figure 5. The maximum strain and recovery ratio vs DCP content in the two-way shape memory behaviors of the cured PCOs under an applied stress (600 kPa).

Extracting the strain increment during cooling from the data sets of Figure 4, we can clearly see the inverse effect of cross-linking density on actuation (Figure 5). In particular, the strain increment increases, under constant stress, from 20% (that is 20% more strain than the background strain for 600 kPa at 100 °C) for PCO-D2.0 to 36% for PCO-D1.0. This result indicates that the strain increment during crystallization increases for samples whose amorphous network chains are already more oriented in the stretching direction due to higher sample compliance. However, evident in Figure 5 is a tradeoff between the strain increment and strain recovery ratio, as we now describe.

The elongation event upon cooling is quite completely reversed through a heat-induced contraction upon heating back to the original temperature (Figure 4), revealing significant hysteresis due to undercooling of the crystallization event. In total, we observe a reversible, two-way, shape memory effect that can be considered a type of thermal actuator. Heating PCO samples that had undergone crystallization under stress, and associated elongation, above their melting temperature melts the crystalline regions, triggering a recovery back to the precrystallization strain for a value of $R_{act}(\sigma)$ close to zero. Figure 5 shows the trend in recovery ratio with DCP content, revealing that values close to 100% are achievable for DCP levels close to 2 wt %. Thus, higher cross-linking produces a more stable rubbery state at high-temperature that is resistant to creep over time and during thermal cycling.

It is expected from rubber elasticity theory that uniaxially loaded elastomers will contract on heating and elongate on cooling; however, this effect is small compared to the crystallization-induced elongation we have observed. Considering elastic effects alone, the constitutive behavior of an elastomer can be adequately explained by considerations of network chain thermodynamics and the number density of network chains. The relationship between extension ratio $f(\lambda)$ and tensile engineering stress (σ) is given by[36]

$$\sigma = NkTf(\lambda) \quad (4)$$

$$f(\lambda) = (\lambda - 1/\lambda^2) \tag{5}$$

$$\lambda = \epsilon + 1 \tag{6}$$

Where N is the number of chains in the network per unit volume, T is absolute temperature, σ is stress, ϵ is strain, and k is Boltzmann's constant. In addition, $f(\lambda)$ is a monotonically increasing function of λ for $\lambda > 1$. When it is assumed that cross-linking density and an applied stress are constant, the relationship between extension ratio $f(\lambda)$ and temperature (T) is as follows.

$$f_L(\lambda) = f_H(\lambda)T_H/T_L \tag{7}$$

where $f_L(\lambda)$and $f_H(\lambda)$ represent the extension ratio at a low and high-temperature, respectively. Equation 7 indicates that the extension ratio is inversely proportional to temperature, in agreement with Figure 4 for the cooling and heating portions above crystallization and melting transitions, respectively. For example, when cooling, the strain increases gradually (1% for every 10 °C as seen in Figure 4), indicating a minor effect of entropy elasticity consistent, at least qualitatively, with classic theory. In stark contrast, a 10× sharper elongation event (∼1% per 1 °C) is witnessed during crystallization and this sharp transition is reversed with nearly the same slope, though at a higher temperature. Thus, both rubber elasticity and our observed crystallization induced elongation contribute to elongation on cooling and contraction on heating, with the crystallization effect being about 10 times sharper.

Increasing the applied load (stress) during actuation was observed to have multiple effects, as revealed in Figure 6 where PCO-D2.0 samples were thermal cycled at different stress levels. While the offset strain increases with applied loads (Supporting Information), the strain increment also increases. For example, Figures 6 and 7 reveal that increasing the applied tensile stress from 500 to 700 kPa (a 40% increase) raised the strain increment from 17.4% to 28.3% (a 62% increase). Extrapolating the strain increment to the stress-axis allowed estimation of a critical stress for PCO-D2.0 of $\sigma_c = 170$ kPa. Below this stress, crystallization-induced elongation is not activated. Important for consideration as actuators, we have also observed that increasing the applied stress shifted the transition temperatures for both elongation and contraction to higher values (especially the crystallization temperature) while slightly decreasing the level of hysteresis (Figure 7). Concerning the melting transition, we postulate that as the stress applied during crystallization is increased comparatively larger and more stable crystallites are formed, leading to a higher melting temperature and associated onset temperature for strain recovery. More specifically, stretching the PCO elastomers under high stress will tend to alter the conformation of the network chains from their equilibrium randomly coiled state to a more extended state, acting as a "seed" to promote extended chain crystallite growth toward a direction parallel to the stretching direction.[37]

To better understand the nature of the PCO crystalline structure formed during cooling under stress, we examined the degree of crystallinity calorimetrically for a range of stresses and with particular attention on PCO-D1.25 as a representative sample. Thus, following cooling-induced crystallization and elongation to $T = 0$ °C, samples were collected from the DMA apparatus and DSC analyses were then performed immediately from −10 to 100 °C at a rate of 10 °C/min. Then, the crystallinity of the stretched samples was determined from the *first* heating scan using DSC to measure endothermic latent heat of melting and dividing the value by the value known for a pure crystal of PCO (216 J/g).[38] (Raw first heat DSCs are available as Supprting Information.) Following this procedure, we found that the degree of crystallinity increased from 30.6% for an applied load of 500 kPa to 34.2% for an applied load of 700 kPa. In addition, the melting point shifted to a slightly higher temperature with increasing stress. After carrying out each first heating scan, the first cooling and second heating scans of the stressed samples were identical to those reported for the unstretched PCO samples (Figure 1), proving that the modification to crystallinity was strictly due to the stress applied during cooling.

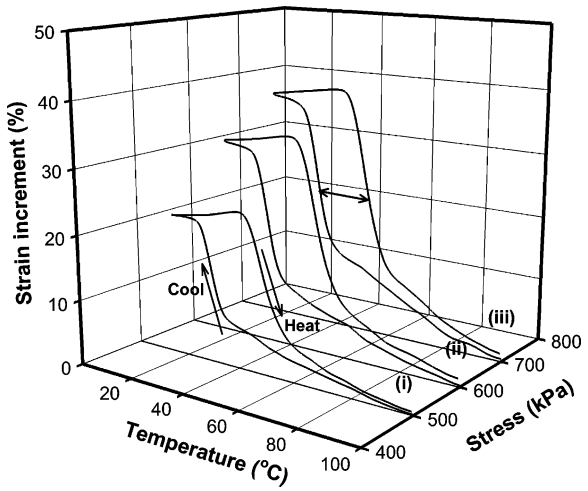

Figure 6. Two-way shape memory behavior for PCO-D2.0 at different stresses, (i) 500, (ii) 600, and (iii) 700 kPa. The samples were deformed at high temperature under each applied stress. The deformation step is followed by cooling and heating processes (2 °C/min) under the constant stress, respectively.

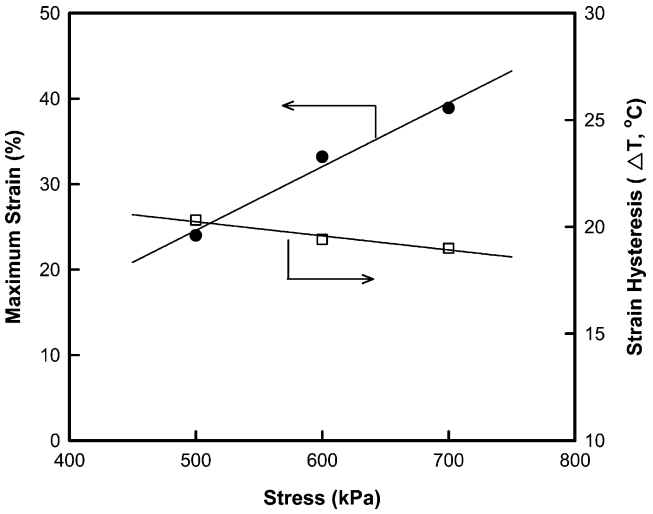

Figure 7. The maximum strain and thermal strain hysteresis vs the applied stress in the two-way shape memory behavior of PCO-D2.0. ● and □ indicate the strain and strain thermal hysteresis, respectively. Thermal strain hysteresis was calculated from the difference of temperature (ΔT) at the half of strain loop generating during cooling and heating as indicated by the bold arrow.

WAXD Analysis. On the basis of the results presented above, we assert that microstructural changes and molecular orientation effects are associated with the unusual two-way shape memory behavior discussed in this investigation. Therefore, two-dimensional wide-angle X-ray scattering patterns were obtained from PCO-D1.5 samples oriented by cooling under load. Samples whose thermomechanical history had been previously erased by subjecting them to 100 °C were collected in the same manner as for DSC (discussed above) for a range of stresses,

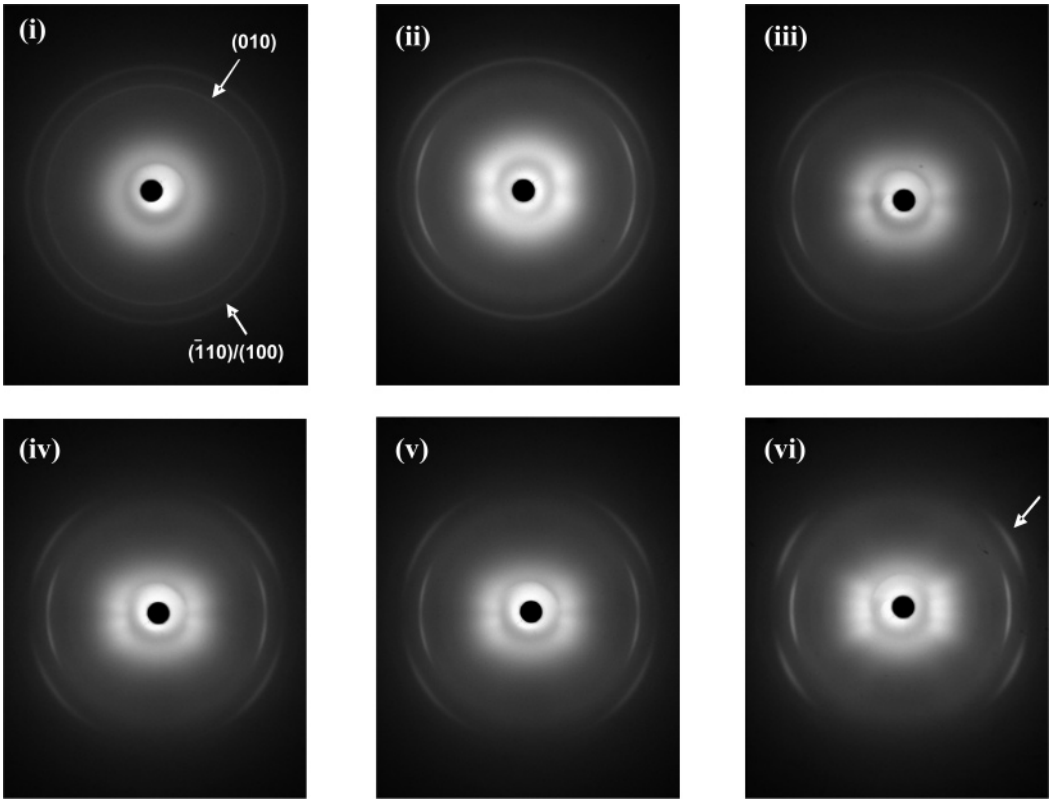

Figure 8. 2D WAXD patterns of the PCO-D1.5 sample with an increase of strain after cooling as a function of the applied stress: (i) unstretched, (ii) 300, (iii) 400, (iv) 500, (v) 600, and (vi) 700 kPa. Drawing direction is vertical.

leading to the patterns shown in Figure 8. It is known that PCO crystallizes in a triclinic or monoclinic microstructure, or a mixture thereof, depending on the conditions of crystallization.[39,40] The unstretched, but thermally cycled, PCO sample (Figure 8i) shows two sharp Debye−Scherrer (crystalline) reflections, whose uniform intensity around the azimuth denotes isotropic chain orientation. The reflections are located at $2\theta = 20.0°$ (4.43 Å) and $2\theta = 23.0°$ (3.85 Å), corresponding to the (010) and $\bar{1}10$ ($\bar{1}00$)/(100) reflections characteristic of a triclinic crystal structure (Figure 8i).

For samples undergoing crystallization-induced elongation at 300 kPa (Figure 8ii), the diffraction pattern becomes anisotropic: the (010) reflection splits into four off-equatorial reflections whereas the ($\bar{1}10$) reflections are azimuthally spread and appear mostly located on the meridional axis. (The equatorial axis is horizontal, and the meridional axis is vertical.) While anisotropy in the diffraction pattern in Figure 8ii denotes preferred orientation, the off-equatorial (010) reflections show that the molecular orientation is neither along the stretching (vertical) direction nor unimodal but rather bimodal. That is, under these stretched conditions there coexist two populations of oriented crystallites. More specifically, a distribution of crystallite orientations exists around $\phi = \pm 16°$ ($\phi = 0°$ along the equatorial axis), as deduced from the azimuthal spread of the (010) reflections. Furthermore, the azimuthal and radial concentration of intensity for the (010) reflections (relative to the unstressed sample) indicates a stress-induced increase in the degree of crystallinity, in agreement with the DSC results discussed above.

On increasing the load during crystallization to 400 kPa (Figure 8iii), the off-equatorial (010) reflections rotate toward the equatorial axis, whereas the ($\bar{1}10$) reflections now split into four off-meridional reflections. At this stress of 400 kPa, the (010) reflections become positioned at $\phi = \pm 13°$. Thus, the larger elongation induced by the 400 kPa stress forces the crystallites to gradually orient toward the stretching direction. Although the sample still exhibits a bimodal orientation, the WAXD pattern in Figure 8iii shows that the azimuthal spread of the (010) reflections has been significantly reduced indicating a narrowing of the distribution of orientation of the crystallites. Figure 8iv shows the WAXD pattern obtained for a sample stretched under a load of 500 kPa. It can be seen that the (010) reflections are now closer to the equatorial axis ($\phi = \pm 9°$) and have started to overlap. On the other hand, the intensity of the ($\bar{1}10$) reflections is now more concentrated azimuthally. Therefore, under this load the network chains have crystallized with crystal orientation closer to the stretching direction.

Although the angular position along the azimuth of the (010) reflections is changing as a function of the applied stress, the angular position in $°2\theta$ (and *d*-spacing) did not change. Therefore, we suggest that the triclinic phase of PCO is unchanged. Tadokoro et al.[41] reported a similar bimodal orientation for a semicrystalline polymer polyvinyl alcohol. These authors showed how the same crystallographic structure can coexist in two different orientations as a result of a given thermomechanical treatment.

Increasing the stretching load continued the reorientation trend of the crystalline structure. Eventually, at the highest stresses applied (600 and 700 kPa), the associated WAXD patterns (parts v and vi of Figure 8, respectively) reveal fiberlike structure. The (010) reflections tend to merge on the equatorial axis, indicative of unimodal crystalline orientation along the stretching direction. The stress-induced transition from bimodal to unimodal orientation is also accompanied by a slight reduction in the width of the (010) reflections (in $°2\theta$, see Supporting Information, and the intensity of the (010) reflection increased, though remaining azimuthally spread, indicating a distribution of molecular orientations along the stretching direction. The reduction of the (010) reflection (in $°2\theta$) indicates that the size

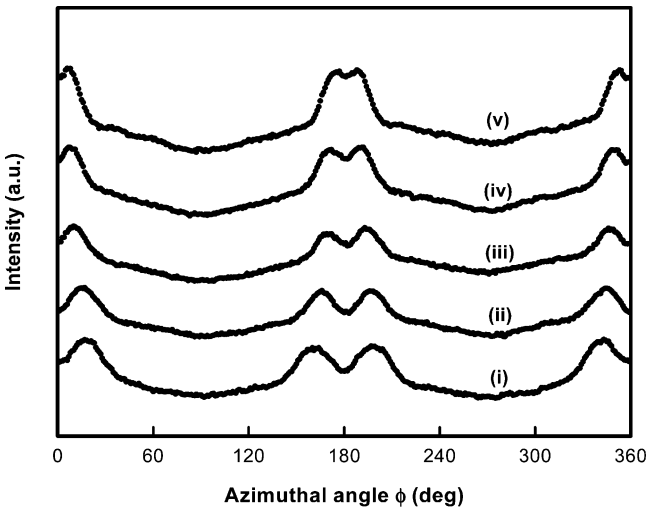

Figure 9. Azimuthal scanning profiles for the (010) reflection of the PCO-D1.5 sample as a function of the applied stress: (i) 300, (ii) 400, (iii) 500, (iv) 600, and (v) 700 kPa.

of crystallites increased as the loading stress increased, and this is consistent with the increase in thermal transitions observed by DSC. Additionally, by increasing the stress the ($\bar{1}10$) reflections are more intense, azimuthally concentrated, and remain off the meridional axis thus forming the first layer along the meridional axis. (arrow in Figure 8vi).

The central area of the patterns shows an amorphous halo that changes upon deformation. It is noted that the presence of a central amorphous halo is very common when using Ni-filtered copper radiation, as the filter cannot eliminate the tail of the white radiation. Consequently, this tail gives rise to a central amorphous halo observed in Figure 8i. Upon deformation, the pattern becomes anisotropic and this is also reflected in the parasitic scattering from the white radiation tail. Thus, the changes observed in the central amorphous halo of the WAXS patterns (Figure 8) are only an experimental artifact.

The degree of molecular anisotropy with deformation was further analyzed by plotting the azimuthal intensity profiles integrated along a narrow band ($\Delta°2\theta$) centered at the (010) reflections as shown in Figure 9. The angles 0° and 180° correspond to the equatorial axis. The intensity profile corresponding to a load of 300 kPa (Figure 9, trace i) shows two pairs of intensity maxima around 0° and 180°. These intensity maxima become azimuthally narrower with increasing stress, an indication of a significant increase in the degree of molecular orientation. Moreover, with increasing stress, the (010) reflections tend to merge into a single peak, indicating that the crystalline microstructure orients increasingly along the stretching direction. As the apparent critical stress for actuation, σ_c, is significantly lower than the stress associated with bimodal-to-unimodal 010 orientation (between 600 and 700 kPa; Figure 9), the two phenomena appear to be uncorrelated.

Mechanically, we have shown further that higher applied stresses (above the "critical stress") during crystallization promote an increase in strain upon cooling (see Figure 6). Considered in light of our X-ray diffraction results (Figures 8 and 9), we can suggest that the elongation during crystallization is associated with (if not caused by) reorientation of crystalline structure toward the stretching direction. As the crystalline structure evolves from bimodal (low stress) to unimodal (high stress), the crystallization occurs along a single preferred orientation thus inducing greater elongation along the stretching direction.

Conclusions

A set of cross-linked PCO samples, an example of a semicrystalline network, was prepared by variation in the concentration of dicumyl peroxide (DCP) used as a thermal initiator in order to investigate two-way shape memory behavior. The thermal and mechanical properties of PCO networks were investigated using differential scanning calorimetry (DSC), gel fraction analysis, dynamic mechanical analysis (DMA), and wide-angle X-ray diffraction (WAXD). We found that the melting (T_m) and crystallization (T_c) temperatures gradually decreased with increasing the concentration of DCP. The gel fractions and rubbery modulus (E') increased with increasing the DCP concentration. Analysis of shape memory properties with a dynamic mechanical analyzer (DMA) revealed that the cured PCOs undergo significant elongation in strain on cooling and contraction on heating under a constant load, revealing novel two-way shape memory behavior in a very simple polymer system. Crystallization induced the strain increment while melting induced contraction. The thermally reversible behavior was affected by the cross-linking density of the PCO network and the stress applied to stretch the PCO chains at high temperature.

WAXD analysis further elucidated the mechanism of crystallization-induced elongation, suggesting that the increase in strain originates from the growth of crystallites oriented along the stretching direction and that the crystallization was promoted increasingly along the uniaxial loading axis with increasing stress, thus resulting in the greater elongation along that direction. As a result, this novel two-way shape memory behavior occurred reversibly through the crystallization-induced elongation in the uniaxial stress direction during cooling and the melting-induced contraction upon heating.

Acknowledgment. P.T.M. acknowledges support for this research by an NSF CAREER Award CTS-0093880 and NSF Grant (DMR-0758631). T.C. acknowledges the support of a graduate fellowship from General Motors Corporation.

Supporting Information Available: Large-strain tensile testing at temperatures, $T > T_m$, reveals quite elastic response of the DCP-cured PCO samples, with stress−strain hysteresis completely removed for PCO-D2.0, raw strain vs temperature plots for the two-way shape memory effect, first-heat DSC traces following crystallization-induced elongation to reveal the degree of crystallinity, and 1D-WAXD patterns for PCO-D1.5 revealing change in peak width with crystallization stress. This material is available free of charge via the Internet at http://pubs.acs.org.

References and Notes

(1) Lendlein, A.; Kelch, S. *Angew. Chem., Int. Ed.* **2002**, *41*, 2034−2057.
(2) Beloshenko, V. A.; Varyukhin, V. N.; Voznyak, Y. V. *Russ. Chem. Rev.* **2005**, *74*, 265−283.
(3) Liu, C.; Qin, H.; Mather, P. T. *J. Mater. Chem.* **2007**, *17*, 1543−1558.
(4) Jeong, H. M.; Lee, S. Y.; Kim, B. K. *J. Mater. Sci.* **2000**, *35*, 1579−1583.
(5) Tobushi, H.; Hara, H.; Yamada, E.; Hayashi, S. *Smart Mater. Struct.* **1996**, *5*, 483−491.
(6) Li, F.; Chen, Y.; Zhu, W.; Zhang, X.; Xu, M. *Polymer* **1998**, *39*, 6929−6934.
(7) Jeon, H. G.; Mather, P. T.; Haddad, T. S. *Polym. Int.* **2000**, *49*, 453−457.
(8) Sakurai, K.; Tanaka, H.; Ogawa, N.; Takahashi, T. *J. Macromol. Sci., Phys.* **1997**, *B36*, 703−716.
(9) Lendlein, A.; Langer, R. *Science* **2002**, *296*, 1673−1676.
(10) Lagoudas, D. C.; Tadjbakhsh, I. G. *Smart Mater. Struct.* **1993**, *2*, 71−81.
(11) Bruck, H. A.; Moore, C. L.; Valentine, T. L. *Smart Mater. Struct.* **2002**, *11*, 509−518.

(12) de Blonk, B. J.; Lagoudas, D. C. *Smart Mater. Struct.* **1998**, *7*, 771−783.
(13) Shenoy, D. K.; Thomsen, D. L., III; Srinivasan, A.; Keller, P.; Ratna, B. R. *Sens. Actuators, A* **2002**, *A96*, 184−188.
(14) Thomsen, D. L., III; Keller, P.; Naciri, J.; Pink, R.; Jeon, H.; Shenoy, D.; Ratna, B. R. *Macromolecules* **2001**, *34*, 5868−5875.
(15) Li, Y.; Hu, Z.; Chen, Y. *J. Appl. Polym. Sci.* **1997**, *63*, 1173−1178.
(16) Pelrine, R.; Kornbluh, R.; Pei, Q.; Joseph, J. *Science* **2000**, *287*.
(17) Pelrine, R.; Kornbluh, R.; Joseph, J.; Heydt, R.; Pei, Q.; Chiba, S. *Mater. Sci. Eng., C* **2000**, *11*, 89−100.
(18) Nam, J. D.; Choi, H. R.; Tak, Y. S.; Kim, K. J. *Sens. Actuators, A* **2003**, *A105(1)*, 83−90.
(19) Otero, T. F.; Sansinena, J. M. *Bioelectrochem. Bioenerg.* **1995**, *38*, 411−414.
(20) Otero, T. F.; Grande, H.; Rodriguez, J. *J. Phys. Org. Chem.* **1996**, *9*, 381−386.
(21) Baughman, R. H. *Synth. Met.* **1996**, *78*, 339−353.
(22) Bay, L.; West, K.; Sommer-Larsen, P.; Skaarup, S.; Benslimane, M. *Adv. Mater. (Weinheim, Ger.)* **2003**, *15*, 310−313.
(23) Lehmann, W.; Skupin, H.; Tolksdorf, C.; Gebhard, E.; Zentel, R.; Kruger, P.; Losche, M.; Kremer, F. *Nature (London, U.K.)* **2001**, *410*, 447−450.
(24) Zhang, Q. M.; Li, H.; Poh, M.; Xia, F.; Cheng, Z. Y.; Xu, H.; Huang, C. *Nature (London, U.K.)* **2002**, *419*, 284−287.
(25) Warner, M.; Terentjev, E. M. *Liquid Crystalline Elastomers*; Oxford University Press: Oxford, U.K., 2003.
(26) Wermter, H.; Finkelmann, H. *e-Polymers* (online computer file, http://www.e-polymers.org)) **2001**, Paper No. 13.
(27) Finkelman, H.; Kock, H. J.; Rehage, G. **1981**, *2*, 317.
(28) Tajbakhsh, A. R.; Terentjev, E. M. *Eur. Phys. J. E* **2001**, *6*, 181−188.
(29) Rousseau, I. A.; Mather, P. T. *J. Am. Chem. Soc.* **2003**, *125*, 15300−15301.
(30) Patil, H. P.; Liao, J.; Hedden, R. C. *Macromolecules* **2007**, *40*, 6206-6216.
(31) Liu, C.; Chun, S. B.; Mather, P. T.; Zheng, L.; Haley, E. H.; Coughlin, E. B. *Macromolecules* **2002**, *35*, 9868−9874.
(32) Liu, C.; Wu, J.; Mather, P. T. *PMSE [Prepr.]* **2003**, *89*, 673−674.
(33) Gao, J.-M.; Lu, Y.; Wei, G.; Zhang, Y.; Qiao, J. L. *J. Appl. Polym. Sci.* **2002**, *85*, 1758−1764.
(34) Jiao, C. M.; Wang, Z. Z.; Liang, X. M.; Hu, Y. *Polym. Test.* **2005**, *24*, 71−80.
(35) Vaughan, A. S.; Zhao, Y.; Barre, L. L.; Sutton, S. J.; Swingler, S. G. *Eur. Polym. J.* **2003**, *39*, 355−365.
(36) Treloar, L. R. G. *The Physics of Rubber Elasticity*, 3rd ed.; Clarendon Press: Oxford, U.K., 1975.
(37) Krigbaum, W. R.; Dawkins, J. V.; Via, G. H.; Balta, Y. I. *J. Polym. Sci., Polym. Phys. Ed.* **1966**, *4*, 475−489.
(38) Schneider, W. A.; Muller, M. F. *J. Mol. Catal.* **1988**, *46*, 395−403.
(39) Natta, G.; Bassi, I. W.; Fagherazzi, G. *Eur. Polym. J.* **1967**, *3*, 339−352.
(40) Bassi, I. W.; Fagherazzi, G. *Eur. Polym. J.* **1968**, *4*, 123−132.
(41) Tadokoro, H.; Seki, S.; Nitta, I. *J. Polym. Sci.* **1958**, *28*, 244−247.

MA071517Z